Supplemental Appendix

Table of contents

Supplemental Table 1. In vivo 3T MRI sequence parameters (patients' screening)

Manufacturer	Philips	Siemens
Precontrast 3D T2-FLAIR sequence		
Repetition time (TR, ms)	4800	4800
Echo Time (TE, ms)	438.6	354
Inversion time (TI, ms)	1600	1800
Flip angle (FA)	90	120
Resolution (mm)	1x1x1	1x1x1
Precontrast 3D EPI T2* sequence		
Repetition time (TR, ms)	54	64
Echo Time (TE, ms)	29.4	35
Flip angle (FA)	10	10
Resolution (mm)	0.55x0.55x0.55	0.65x0.65x0.65
Pre and postcontrast 3D T1-MPRAGE sequence		
Repetition time (TR, ms)	7.6	7.8
Echo Time (TE, ms)	2.4	3
Inversion time (TI, ms)	900	900
Flip angle (FA)	18	18
Resolution (mm)	1x1x1	1x1x1

Abbreviations: EPI, echo planar imaging.

Supplemental Figure 1. Non-uniform susceptibility of the persistent phase rim in cortical/juxtacortical lesions

Longitudinal susceptibility changes in cortical/juxtacortical lesions in two cases of relapsing-remitting multiple sclerosis (A and B correspond, respectively, to patients #1 and #5 in Table 1). At baseline, the thickness and signal intensity of the phase rim in the centripetally enhancing lesion were homogeneous on phase images. During the follow up, the persistent rim was qualitatively more prominent on both T2*-weighted magnitude and phase images (red arrows) at the white/gray matter junction (A, B) and intracortically (B) compared to the subcortical white matter. These susceptibility findings were present at month 12 in A and much earlier in B (month 3).

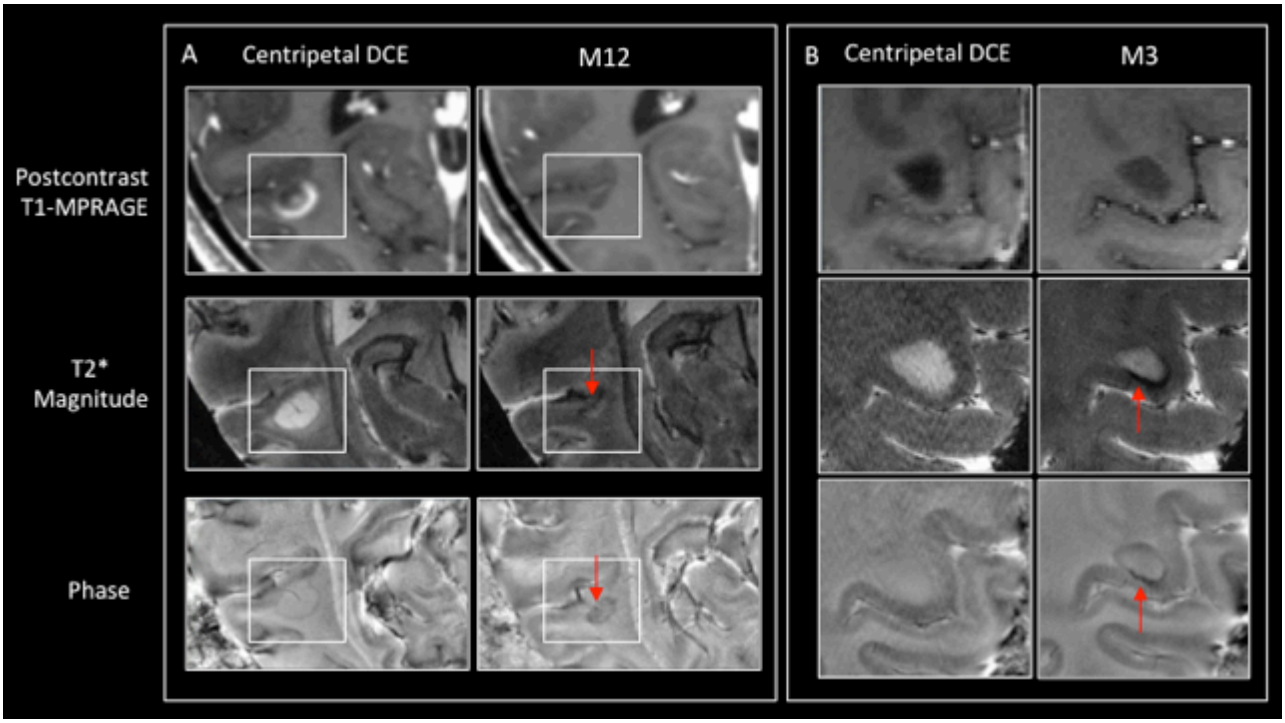

Peripheral cytokine/chemokine profile at the time of radiological relapse and after one year

Results. Since we observed three groups of lesion according to dynamic contrast enhancement and phase rim patterns, we conducted an exploratory linear discriminant analysis in order to assess whether the cytokine/chemokine profile in the peripheral blood was also able to distinguish samples into three groups. We found that the first discriminant function tended to separated centripetal from centrifugal lesions (Wilks's lambda=0.03, p=0.12). Score plots on the plane of the two discriminant functions for all samples, separated according to time point (baseline vs. month 12), are shown in Supplementary Figure 2. The cytokine/chemokine peripheral profile was able to classify correctly 92% of cases as originally grouped. In general, Th1-polarized inflammatory cytokines (IL12, IFNγ, CXCL10, IL2, IL15) correlated better with centripetal lesion groups than with their centrifugal counterparts (Supplementary Figure 2), with the exception of the anti-inflammatory cytokine IL10. Repeated-measures ANOVA of both discriminant function scores showed significant interaction between lesion groups and time points (p=0.01 and 0.04, respectively), with reduced group-wise mean differences at follow-up where the centroids were closer to 0.

Methods. In this exploratory analysis in 10 participants, peripheral blood samples were collected at baseline (radiological relapse) and after one year (remission) and stored at −80° until use. Chemokine and cytokine profiles were evaluated using a V-PLEX Human Cytokine 30-plex Kit (Meso Scale Discovery). All serum samples were run in triplicate at dilutions in accordance with the manufacturer's instructions. Analytes were retained in the final statistical analysis only if above the lower limit of detection (LLOD) for a given analyte. The LLOD is a concentration corresponding to a signal 2.5 standard deviations above the zero calibrator. No samples exceeded the upper limit of quantification. The following analytes entered the statistical analysis: IP10 (CXCL10), MCP1 (CCL2), MCP4 (CCL13), MDC, MIP-1b (CCL4), TARC (CCL17), IL12, IL15, IL16, IL7, VEGF, IFNγ, IL2, IL6, IL10, TNFα, IL8. A linear discriminant analysis was performed in order to assess whether the peripheral cytokine/chemokine profile could discriminate samples according to three lesion groups (centrifugal, centripetal with transient phase rim, and centripetal with persistent phase rim). The first discriminant function separated centripetal from centrifugal lesions, while the second discriminant function centripetal lesions with transient vs. persistent rim. Repeated-measures ANOVA evaluated discriminant function scores across groups at baseline and month 12.

Supplemental Figure 2. (A) Scores on the two discriminant functions and group centroids (solid symbols) for all samples showing time point (open symbols for baseline and shaded symbols for year 1). Lesion groups are color-coded: centrifugal lesions in red, centripetal lesions with transient rim in green, centripetal lesions with persistent rim in blue. Baseline samples contributed the most to the group differentiation (month 12 group

centroids closer to 0). (B) Plot of each cytokine/chemokine's loading on the two discriminant functions (predominantly pro-inflammatory cytokines, red squares; anti-inflammatory cytokines, green diamond; chemokines, black circles; lymphocyte differentiation cytokines, blue triangle). In general, centripetal lesion groups positively correlated with pro-inflammatory cytokines, although there are some exceptions (mainly IL10).

Abbreviations: F1: discriminant function 1; F2: discriminant function 2.

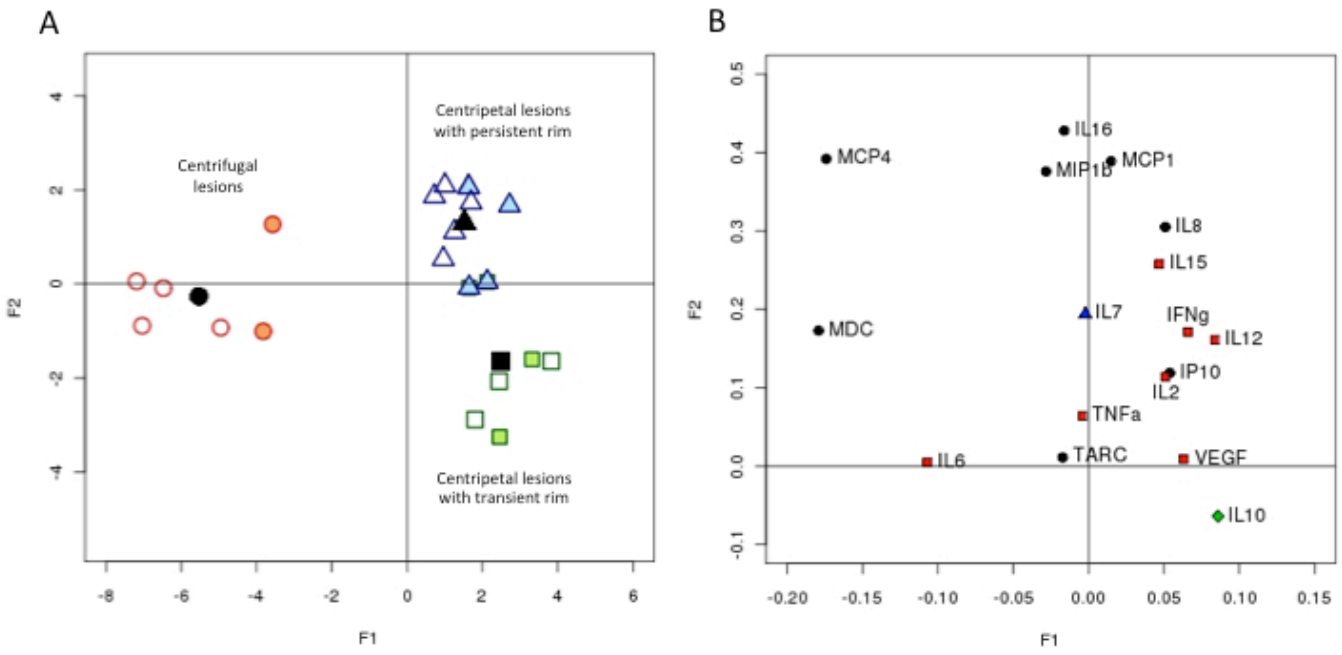

Neuropathological evaluation

Autopsy cases

Progressive MS patients	Age at death (years)	Cause of death	Histological lesion analysis	Lesions with phase rim on postmortem MRI
#1 (male)	59	Brainstem stroke	4 tissue blocks (3 periventricular and 2 leukocortical lesions)	Positive
#2 (female)	68	Natalizumab-associated progressive multifocal leukoencephalopathy (brainstem-cerebellum)	2 tissue blocks (2 periventricular lesions)	Negative
#3 (female)	60	Sepsis	4 tissue blocks (2 periventricular, 1 deep WM and, 1 juxtacortical)	Negative

The clinical and radiological history of Patient #1 have been previously described in Absinta et al., Neurology 2015 (Supplemental Data). This patient underwent an in vivo 7T MRI scan in June 2012. The protocol was the same used for the in vivo patient cohort in this paper.

Postmortem 7-tesla MRI. Postmortem MRI was performed on the same 7T MRI scanner. The following sequences were executed on all formalin-fixed whole brains:

1. 3D T1-weighted magnetization-prepared rapid gradient echo (T1-MPRAGE) with repetition time (TR) = 2200 ms; echo time (TE) = 3.04 ms; inversion time (TI) = 1050 ms; flip angle (FA) = 7°; nominal resolution = 0.6x0.6x0.6 mm; and 176 coronal slices. The acquisition time for the sequence was 6 min 35 sec.
2. 3D high-resolution multigradient-echo (GRE) T2* sequence providing both T2*-weighted magnitude contrast and susceptibility-weighted phase contrast: TR = 60 ms; TE = 6.09, 15.99, 25.89, 35.79 ms; 4 averages; 88 slices; FA = 10°; acquisition time = 2 hours 15 min per 36 mm slab; nominal resolution =

0.42x0.42x0.42 mm. Four coronal slabs with 20% overlapping slices were acquired to cover the whole brain.

All imaging slices were aligned parallel to a plane passing through the mammillary bodies. Images acquired in multiple slabs covering the whole brain were stitched together using the embedded information in the image files and post-processing algorithms developed using the AFNI software package.

Tissue sampling. Following postmortem whole-brain 7T MRI, brain sectioning was performed using an individualized, MRI-designed, 3D-printed cutting box for fixed brain. Details relative to this device and the sectioning procedure have been previously described (Absinta et al., 2014). The tissue sampling was MRI-guided. Tissue blocks and relative demyelinated lesions were selected because of the presence or absence of a paramagnetic rim as detected on in vivo and/or postmortem images.

Histology. Eight of ten formalin-fixed tissue blocks were embedded in paraffin. The remaining 2 formalin-fixed tissue blocks were immersed in 30% sucrose at 4 °C for ~2 days for cryoprotection and then embedded with Optimal Cutting Temperature (Tissue-Tek OCT, Sakura, Torrance, CA, USA) compound for freezing and sectioning. 5- or 10-µm sections were obtained on a sliding microtome and mounted on 1x3-inch glass slides. Slides were prepared with hematoxylin and eosin (H&E), Luxol fast blue/periodic acid Schiff (LFB-PAS), Bielschowsky's method, and diaminobenzidine (DAB)-enhanced Turnbull staining. Stained sections were digitized at 20× magnification using a slide scanner (iScan Coreo, Ventana Medical Systems, Inc., Tuscon, AZ, USA) as well a microscope (Axio Observer Z.1, Carl Zeiss Microscopy, NY, USA) and compared with the MRI from the same location. LFB-PAS-stained sections were used for assessment of myelination. Bielschowsky-stained sections were used for axonal integrity assessment DAB-Turnbull for iron assessment.

The DAB-Turnbull staining protocol was performed as follows. Sections were immersed in 2% ammonium sulfide solution for 90 min, then washed with dH2O. Sections were incubated with 10% potassium ferrocyanide solution and 0.5% hydrochloric acid solution at temperature 37C (oven) for 15 minutes. After washing in dH2O five times x3 minutes, sections were incubated in 0.3% H2O2 in methanol for blocking endogenous peroxidase. After washing in PBS, iron staining was amplified by DAB solution (Abcam, #ab94665). After washing, sections were counterstained with 10% hematoxylin.

Immunohistochemistry. Immunostaining was performed on 5 or 10 µm-thick consecutive sections with antibodies to CD68, CD3, CD4, CD8, CD20, CD163, myelin/PLP, ASPA, OLIG2, GFAP and SMI32 (Supplementary Table 2) and visualized with DAB. Briefly, sections were rinsed in triphosphate-buffered saline (TBS) for 10 min

each and then processed for antigen retrieval (Supplementary Table 2) followed by treatment in 0.3% hydrogen peroxide for 10 minutes. The sections were blocked with a protein blocking solution for 20 minutes and incubated with the primary antibodies overnight at 4C or 1 hour room temperature (Supplementary Table 2), then rinsed and incubated with secondary antibodies for 30 minutes. The immunoreaction was visualized with DAB. After washing, sections were counterstained with 10% hematoxylin.

Double staining. ASPA/OLIG2 and CD163/CD68 double staining was performed using, in sequence, DAB horseradish peroxidase (HRP) and Vector Blue alkaline phosphatase (AP) methods. DAB-Turnbull/CD68 and DAB-Turnbull/GFAP double staining was performed using, in sequence, DAB-Turnbull staining and then Vector Blue AP method.

Supplemental Table 2. Primary antibodies used for immunohistochemistry

Antigen	Target	Primary antibody type	Antigen retrieval	Dilution	Incubation	Source (catalogue #)
CD68	Macrophages/activated microglia	Mouse IgG3 monoclonal	Steamer 45 min	1:100	1 hour RT	Dako (#M087629-2)
CD3	T lymphocytes	Rabbit polyclonal	Steamer 45 min	1:100	Overnight 4C	Dako (#A045229-2)
CD8	CD8 T lymphocytes	Mouse monoclonal	Steamer 45 min	1:100	Overnight 4C	Dako (#M710301-2)
CD4	CD4 lymphocytes	Mouse monoclonal	Steamer 45 min	1:100	Overnight 4C	Dako (#M731001-2)
CD20	B lymphocytes	Mouse monoclonal	Steamer 45 min	1:100	Overnight 4C	Dako (#M075501-2)
CD163	Mature tissue macrophages (inflammation resolution)	Mouse monoclonal	Steamer 45 min	1:100	1 hour RT	AbD serotec (#MCA1853)
Myelin/PLP	Myelin	Mouse monoclonal	Steamer 45 min	1:500	1 hour RT	Courtesy of Prof. Bruce Trapp (Lerner Research Institute, Cleveland, USA)

ASPA	Mature oligodendocytes	Rabbit polyclonal	Steamer 45 min	1:1000	1 hour RT	GeneTex (#GTX113389) (courtesy of Prof. Brian Popko, Universiy of Chicago, Chicago, USA)
OLIG2	Oligodendrocytes precursors>mature oligidendrocytes	Rabbit polyclonal	Pressure cooker 10 min	1:200	1 hour RT	EMD Millipore (#AB9610)
GFAP	Astrocytes	Rabbit polyclonal	Proteinase K	1:100	1 hour RT	Dako (#Z033401-2)
SMI32	Axonal non-phosphorylated neurofilaments H	Mouse monoclonal	Steamer 45 min	1:100	1 hour RT	Biolegend (#801701)

Abbreviations: IHC, immunohistochemistry; RT, room temperature; PLP, proteolipid protein; ASPA: aspartoacylase; GFAP, glial fibrillary acidic protein.

Supplemental Figure 3. MRI-pathology of demyelinated lesions with persistent phase rim (lesion #4)

In vivo and postmortem 7T MRI. In vivo and postmortem 7T MRI showed a leukocortical lesion with a phase rim visible both in vivo (top left) and postmortem (not shown).

Histopathology. Similar to the other analyzed lesions with phase rim, an extensive demyelinating CD68-positive cellular infiltrate is clearly detected at the white matter lesion edge (red arrows) but not in the cortex.

Graph of cell distribution. CD8-positive T lymphocytes and CD68-macrophages/microglia were more prevalent at the lesion edge than in the lesion center and surrounding white matter (mean ± SEM). A mixed population of macrophages/microglia (iron-positive and CD163-positive) was seen at the lesion edge.

* refers to $p<0.0001$ in both edge *vs* center and edge *vs* white matter (ANOVA, post-hoc analysis and Bonferroni correction for multiple comparisons);

& refers to $p<0.0001$ in only edge *vs* center (ANOVA, post-hoc analysis and Bonferroni correction for multiple comparisons).

The numbering of the pathology lesions corresponds to those in Figure 8.

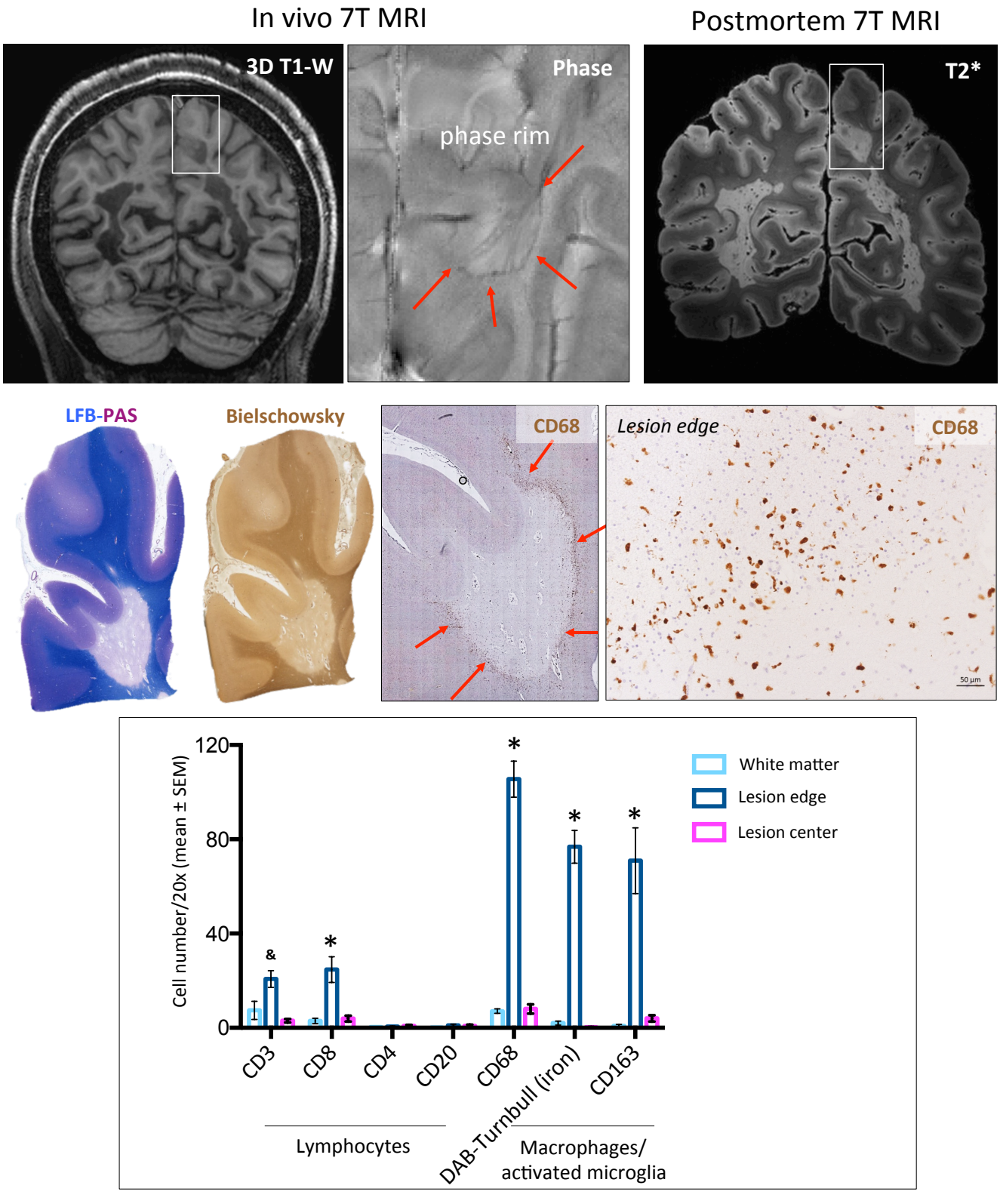
In vivo 7T MRI
Postmortem 7T MRI
3D T1-W
Phase
phase rim
T2*
LFB-PAS
Bielschowsky
CD68
Lesion edge
CD68
50 µm
Cell number/20x (mean ± SEM)
120
80
40
0
&
*
*
*
*
CD3
CD8
CD4
CD20
CD68
DAB-Turnbull (iron)
CD163
Lymphocytes
Macrophages/
activated microglia
White matter
Lesion edge
Lesion center

Supplemental Figure 4. MRI-pathology of demyelinated lesions without phase rim (Lesion #6)

Demyelinated lesions without phase rim did not show a CD68-positive infiltrate at the lesion edge. Even though sparse CD68-positive cells were seen throughout the lesion and in the surrounding white matter, they were not iron-laden (negative DAB-Turnbull staining). The numbering of the pathology lesions corresponds to those in Figure 8.

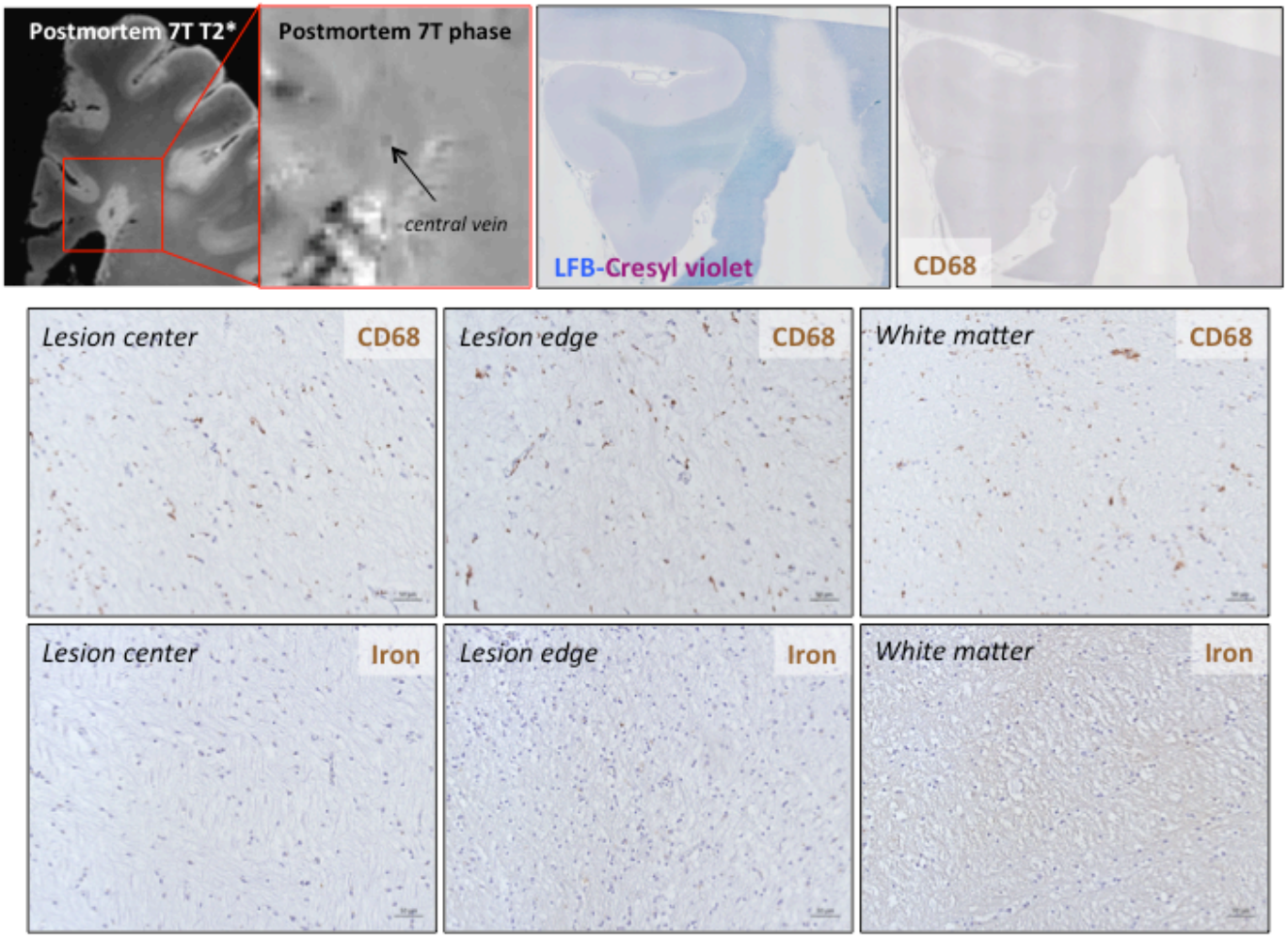

References

Absinta M*, Vuolo L*, Rao A, Nair G, Sati P, Cortese IC, Ohayon J, Fenton K, Reyes-Mantilla MI, Maric D, Calabresi PA, Butman JA, Pardo CA, Reich DS. Gadolinium-based MRI characterization of leptomeningeal inflammation in multiple sclerosis. Neurology. 2015 Apr 17.

Absinta M*, Nair G*, Filippi M, Ray-Chaudhury A, Reyes-Mantilla MI, Pardo CA, Reich DS.
Postmortem magnetic resonance imaging to guide the pathologic cut: individualized, 3-dimensionally printed cutting boxes for fixed brains. J Neuropathol Exp Neurol. 2014 Aug;73(8):780-8.

Absinta M, Sati P, Gaitán MI, Maggi P, Cortese IC, Filippi M, Reich DS. Seven-tesla phase imaging of acute multiple sclerosis lesions: A new window into the inflammatory process. Ann Neurol. 2013 Nov;74(5):669-78.